



Enhancement of plasmonic activity by Pt/Ag bimetallic nanocatalyst supported on mesoporous silica in the hydrogen production from hydrogen storage material

Priyanka Verma ^a, Kaile Yuan ^a, Yasutaka Kuwahara ^{a,b}, Kohsuke Mori ^{a,b,c},
Hiromi Yamashita ^{a,b,*}

^a Division of Materials and Manufacturing Science, Graduate School of Engineering, Osaka University, 2-1 Yamadaoka, Suita, Osaka 565-0871, Japan

^b Unit of Elements Strategy Initiative for Catalysts & Batteries, Kyoto University, Kyoto 606-8501, Japan

^c JST, PRESTO, 4-1-8 Honcho, Kawaguchi, Saitama, 332-0012, Japan

ARTICLE INFO

Article history:

Received 30 September 2016

Received in revised form 27 April 2017

Accepted 4 May 2017

Available online 4 May 2017

Keywords:

Plasmonic catalyst

Bimetallic nanoparticles

Mesoporous silica

Hydrogen production

Ammonia borane

ABSTRACT

Recent advancements in plasmonic catalysis have witnessed rapid developments in solar-to-chemical energy conversion utilizing Ag, Au and Cu metal nanoparticles (NPs). In this study, visible light responsive bimetallic Pt/Ag nanocatalyst supported on mesoporous silica, was successfully prepared by a two-step method viz. MW assisted alcohol reduction, followed by Pt deposition by the assistance of localized surface plasmon resonance (LSPR) effect of Ag NPs. The obtained catalysts were characterized by UV-vis, transmission electron microscopy (TEM), XAFS, XPS and N₂-physisorption measurement studies. The performance of prepared catalysts was explored for the visible light enhanced catalytic activity in the hydrogen (H₂) production from ammonia borane (NH₃·BH₃: AB). A great enhancement for Pt(0.25)/Ag/SBA-15 (0.25 wt% of Pt on 1.0 wt% of Ag) was observed by a factor of 2.8, which is highest among our previously reported results of spherical bimetallic NPs. A plausible photocatalytic and charge separation mechanism has been proposed to envisage the tentative reaction pathway.

© 2017 Elsevier B.V. All rights reserved.

1. Introduction

The perpetual advancements in nanofabrication and nanoparticle (NP) synthesis technologies are leading to the birth of innumerable applications of plasmonics in many different research fields and hence making it as one of the most dynamic and fascinating branch of nanophotonics [1–3]. In the past two decades, the surface plasmons of noble metals have fuelled immense research activities and its applications in surface-enhanced spectroscopies [4], bio sensing [5], lasers [6], photovoltaics [7] and photocatalysis [8]. The tremendous efforts and recent advancements have already witnessed a new insight to the fundamentals of plasmonic systems [9]. Recently, it has been identified as a powerful tool to combine optics with nanoscience and nanotechnology, enabling control of hot charge carriers by manipulating light absorption within femtoseconds at nanoscale regimes [9,10]. The direct photocatalytic

reactions are driven by noble metal NPs due to the presence of accessible active sites and generation of hot electrons by localized surface plasmon resonance (LSPR) effect [11,12]. A myriad of preparative methods have been developed till now to synthesize metal NPs of different size and morphology viz. sphere [13], rods [14], cubes [15] and prisms [16]. The synthesis of Au-Ag alloyed nanoboxes (hollow interior) and nanocages (porous walls) reported recently is one of the example to demonstrate the composition control of NPs [17]. As per recent report from Yuan Li group, the theoretical calculations depict the presence of a special plasmonic resonance (SPR) mode at the interphase of bimetallic core shell structure, in addition to the ordinary mode at surface [18].

Bimetallic nanostructures have attracted significant attention due to their unique optical, catalytic, electronic, magnetic properties in comparison to monometallic and bulk metal alloys [19]. The enhanced performance of bimetallic NPs can be rationalized by electronic (charge transfer), geometric and synergistic effects [20]. Variety of approaches has been reported till date to synthesize bimetallic NPs viz. polyol process [21], wet chemical [22], galvanic [23], electrochemical [24], photochemical [19] or LSPR-assisted deposition [13]. The development of highly dispersed bimetallic NPs supported on mesoporous materials provides an opportunity

* Corresponding author at: Division of Materials and Manufacturing Science, Graduate School of Engineering, Osaka University, 2-1 Yamadaoka, Suita, Osaka 565-0871, Japan.

E-mail address: yamashita@mat.eng.osaka-u.ac.jp (H. Yamashita).

to design catalytically-active advanced functional materials. In continuation of our previous studies on bimetallic plasmonic systems [13,14,25], herein, we report the synthesis of Pt/Ag NPs supported on silica. The quest of developing more and more active and visible light efficient catalytic systems motivated us to study the combination of most active metals of transition series. Significant efforts have already been made to study the combination of Pt/Au NPs, but Pt/Ag combination is still not so well known in exploration of plasmonic effect of Ag in combination with Pt [26].

The growing threat of energy exhaustion and global warming makes the development of sustainable and clean energy production extremely urgent. Hydrogen (H_2) has been regarded as one of the most qualified candidates in terms of its clean burning and high energy density [27]. However, the difficulty in storage and transportation limits its widespread application [28,29]. Recently, ammonia borane ($NH_3\text{-BH}_3$, AB) has received immense attention as a hydrogen storage material owing to its high hydrogen content (19.6 wt%), low molecular weight (30.87 g mol^{-1}), non-toxicity and high stability at room temperature [30]. Therefore, H_2 production from AB was employed a model reaction to compare the catalytic activities of the prepared catalysts under dark and visible light irradiation.

2. Experimental

2.1. Materials

Tetraethyl orthosilicate ($(C_2H_5O)_4Si$), hydrochloric acid (HCl), 1-hexanol ($C_6H_{13}OH$), acetone, silver nitrate ($AgNO_3$), Chloroplatinic acid (H_2PtCl_6), sodium laurate, and ethanol were purchased from Nacalai Tesque Inc. Triblock pluronic P123[®] ($M_w = 5800$, $PEO_{20}PPO_{70}PEO_{20}$) and ammonia borane ($NH_3\text{BH}_3$) were obtained from Sigma-Aldrich Co. All chemicals were used as received without any further purification.

2.2. Synthesis of SBA-15

Mesoporous silica SBA-15 was synthesized according to the method reported in literature utilizing Pluronic P123[®] as a structure directing agent and tetraethyl orthosilicate (TEOS) as a silica source under acidic conditions ($pH < 1$) [31].

2.3. Synthesis of Ag/SBA-15

The incorporation of Ag (1 wt%) onto SBA-15 (0.396 g) was carried out by microwave assisted alcohol reduction method. At first, the silica support was ultrasonicated well with 1-hexanol (40 mL) for 30 min. Further, sodium laurate (surface directing agent, 10 mg) and precursor $AgNO_3$ aqueous solution (100 mmol, 0.4 mL) was injected into the solution followed by Ar bubbling for 15 min. The resultant mixture was then exposed to microwave irradiation (500 W) for a period of 3 min. The solution was then filtered and dried in air at 80 °C. The obtained catalyst was named as Ag/SBA-15.

2.4. Synthesis of Pt/Ag/SBA-15

Four different weight percentages of Pt (0.1, 0.25, 0.5 and 1.0 wt%) was deposited onto Ag/SBA-15 by plasmon-mediated deposition method under visible light irradiation. 0.1 g of Ag/SBA-15 was suspended and ultrasonicated in water (20 mL) until it becomes a clear solution. It was followed by bubbling Ar gas for a period of 30 min to ensure complete inert atmosphere. Subsequently, varying amounts of H_2PtCl_6 solution (1.5 mM) was injected into the reaction mixture and irradiated with a Xe lamp (500 W; San-Ei Electric Co. Ltd. XEF-501S) with continuous stirring for 2 h. The Pt ions were further reduced by employing

hydrazine (N_2H_4) as a reducing agent. The resultant mixture was centrifuged, washed with distilled water and acetone and dried in vacuum overnight at room temperature. The obtained catalysts were denoted as Pt(x)/Ag/SBA, where x represents the weight percentage amount of Pt on Ag.

2.5. Characterization

The overall characterization of the prepared support and catalysts was established by UV-vis, N_2 physisorption, transmission electron microscopy (TEM), and X-ray photoelectron spectroscopic (XPS) analysis. Shimadzu UV-2450 spectrophotometer was used to collect the reflectance UV-vis spectra of powdered samples. $BaSO_4$ was used as a reference solid and the spectra were collected by employing Kubelka-Munk function. Brunauer-Emmett-Teller (BET) surface area measurements were performed by using a BEL-SORP max system (MicrotracBEL) at 77 K. Degassing of the samples was done in vacuum at 473 K for 3 h in order to remove the adsorbed impurities. TEM micrographs were obtained with a Hitachi Hf-2000 FE-TEM equipped with Kevex energy-dispersive X-ray detector operated at 200 kV. ESCA-3400 electron spectrometer was used to characterize samples for X-ray photoelectron spectroscopy. Ag K-edge XAFS spectra were recorded in fluorescence-yield collection technique mode at the beam line 01B1 station with an attached Si (111) monochromator (2016A1095). XAFS data were examined using the REX2000 program (Rigaku).

2.6. Catalytic reaction

The catalytic reaction of dehydrogenation of AB was carried out in an aqueous suspension of catalysts. Briefly, 20 mg of catalyst was dispersed in distilled water (5 mL) in a Pyrex vessel (32 mL), sealed with a rubber septum. After bubbling Ar gas for 30 min, AB (20 μmol) was injected through the rubber septum and stirred continuously under either dark conditions or photo irradiation (320 mW cm^{-2}). A 500 W Xenon lamp (San-Ei Electric Co. Ltd. XEF-501S) was used to carry out reactions under visible light irradiation. The amount of hydrogen in the gas phase was measured by using Shimadzu GC-14B gas chromatograph equipped with a TCD detector.

3. Results and discussions

3.1. Characterization results

3.1.1. TEM measurement

Fig. 1 shows the TEM micrographs along with their pertinent histograms and diagrammatic illustration for Ag and Pt/Ag NPs supported on mesoporous silica (SBA-15). SBA-15 displayed well-ordered mesoporous structure (as seen in TEM), which was further confirmed by low-angle X-ray diffraction (XRD) and N_2 physisorption measurement studies as discussed later. The mean diameter of NPs was found to be approximately 3.18 and 4.15 nm for Ag and Pt/Ag NPs respectively, with a narrow size distribution. MW assisted process for the synthesis of Ag NPs was found to be very efficient in growing NPs within the hexagonal channels of mesoporous silica. After Pt deposition, there observed no specific change in the morphology of Ag NPs, however slight size increment was observed for PtAg bimetallic NPs.

3.1.2. UV-vis absorption measurement

To design plasmonic nanostructures with efficient visible light sensitivity, it is essential to display distinct absorption along with high catalytic performance. Till date, synthesizing NPs with uniform shape and narrow size distribution, exhibiting intense absorption in the visible region is still a great challenge. In order

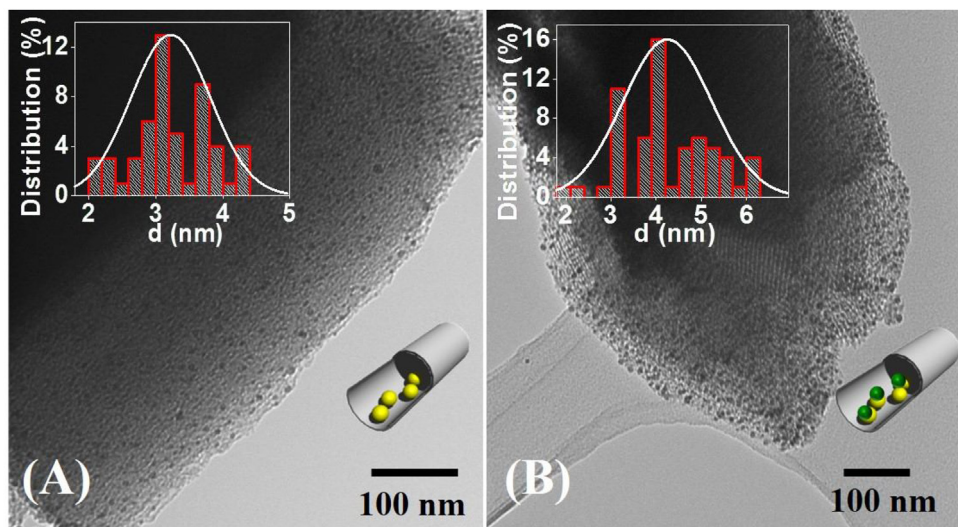


Fig. 1. TEM micrographs along with pertinent histograms for (A) Ag/SBA-15 and (B) Pt(0.25)/Ag/SBA-15.

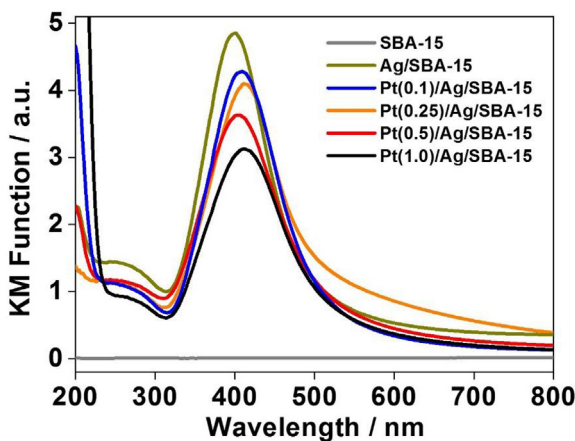


Fig. 2. UV-vis spectra of prepared catalysts.

to characterize the prepared catalysts, surface plasmon resonance (SPR) property was investigated by diffuse reflectance UV-vis absorption spectroscopy. The morphological shape and size of NPs can affect the intensity and wavelength of LSPR peak in the spectrum. Also, the number of LSPR peaks are dependent on the different polarization modes arising from different shapes of metal NPs. For example spheres, rods and cubes gives rise to one, two and three peaks in the UV-vis spectrum respectively. Fig. 2 shows the UV-vis spectra of prepared catalysts including SBA-15 (mesoporous silica), Ag/SBA-15 and Pt(x)/Ag/SBA-15 (where x = 0.1, 0.25, 0.5, 1.0 represents the weight percentage ratio of Pt deposited on Ag). All catalysts exhibited one intense plasmonic peak at wavelength range of 420 nm, also indicating the spherical shape NPs. The presence of the plasmonic peak even after the incorporation of second metal (Pt) confirmed the retention of plasmonic behavior in all prepared catalysts. The continuous decrease in the intensity of Ag plasmonic peak on increasing the Pt weight% ratio, confirms the surface coverage of Ag by Pt. The Ag and Pt/Ag samples were found to be yellow colored, evidently explaining the strong absorption in the visible region.

3.1.3. *N₂* adsorption-desorption measurement

To further characterize the mesoporous structure of the materials, N₂-physisorption measurement studies were carried out. All catalysts exhibited typical H1-type hysteresis loop with a sharp

Table 1
Textural properties determined by N₂-physisorption measurements.

| Materials | Surface area (m ² g ⁻¹) | Pore size (nm) | Pore volume (cm ³ g ⁻¹) |
|--------------------|--|----------------|--|
| SBA-15 | 671 | 9.49 | 1.1 |
| Ag/SBA-15 | 571 | 8.86 | 0.98 |
| Pt(0.1)/Ag/SBA-15 | 508 | 10.18 | 1.02 |
| Pt(0.25)/Ag/SBA-15 | 490 | 9.49 | 0.79 |
| Pt(0.5)/Ag/SBA-15 | 527 | 9.49 | 0.87 |
| Pt(1.0)/Ag/SBA-15 | 466 | 8.86 | 0.91 |

inflexion at pressure range of 0.7 in their isotherms as shown in Fig. S1. The pore size distribution has also been represented in Fig. S2. The detailed textural properties including surface area, pore size and pore volume has been summarized in Table 1. The surface area and mesoporous volume of SBA-15 decreased from 671 to 571 m² g⁻¹ and 1.1 to 0.98 cm³ g⁻¹ respectively for Ag/SBA-15, while 671 to 490 m² g⁻¹ and 1.1 to 0.79 cm³ g⁻¹ respectively for Pt(0.25)/Ag/SBA-15. The successive decrease observed on increasing the Pt weight percentage, in the pore volume and surface area indicates the occupancy of void spaces by NPs.

3.1.4. XAFS analysis

The Ag K-edge X-ray absorption near-edge structure (XANES) spectra of Ag/SBA-15, Pt/Ag/SBA-15, Ag foil and AgO is represented in Fig. 3(A). The observable two peaks and edge position of Ag foil resembles to Ag/SBA-15 and Pt/Ag/SBA-15, but differ from the peak spectra of AgO. Hence, the prepared catalysts possess similar electronic properties and Ag in zero oxidation state. Also, the white line, which is the characteristic small peak for Ag after the edge jump was observed. The slight decrease in the intensity after the deposition of Pt is suggestive of the interaction between Pt and Ag. The magnified XANES spectra of Ag and Pt/Ag SBA-15 is shown in Fig. S3 [32,33].

Extended X-ray absorption fine structure (EXAFS) measurement studies were carried out to elucidate the local structure of NPs supported on mesoporous silica. Fig. 3(B) shows the Ag K-edge Fourier transforms (FT) EXAFS spectra for Ag/SBA-15 and Pt/Ag bimetallic catalyst along with standard samples including Ag foil and Ag oxide (AgO). All samples exhibited an intense peak at 2.7 Å attributed to the contiguous Ag–Ag metallic bonding, similar to that of Ag foil. This confirms the presence of Ag⁰ species in Ag and bimetallic Pt/Ag samples. The recognizable different peak at approximately 1.9 Å for AgO represents Ag–O–Ag bonding.

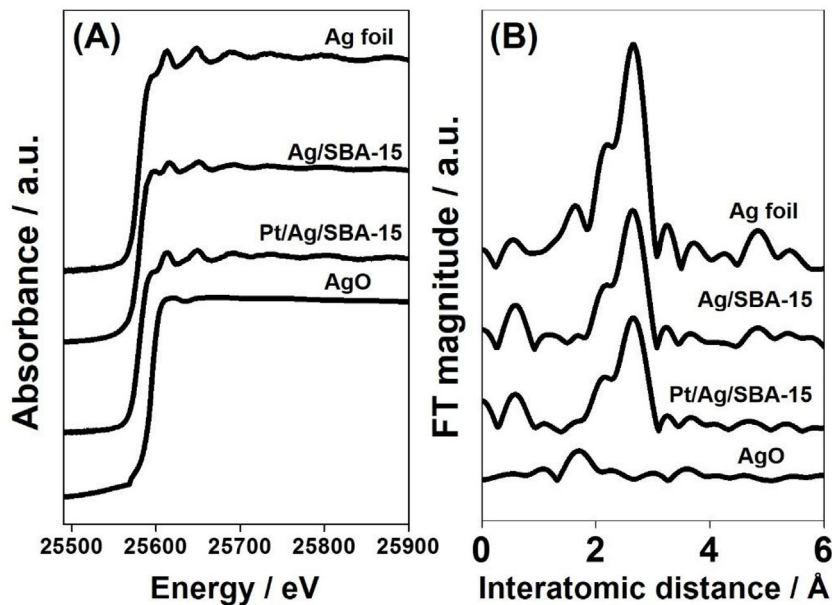


Fig. 3. (A) Ag K-edge XANES spectra and (B) FT-EXAFS for Ag/SBA-15, Pt/Ag/SBA-15, Ag foil and AgO.

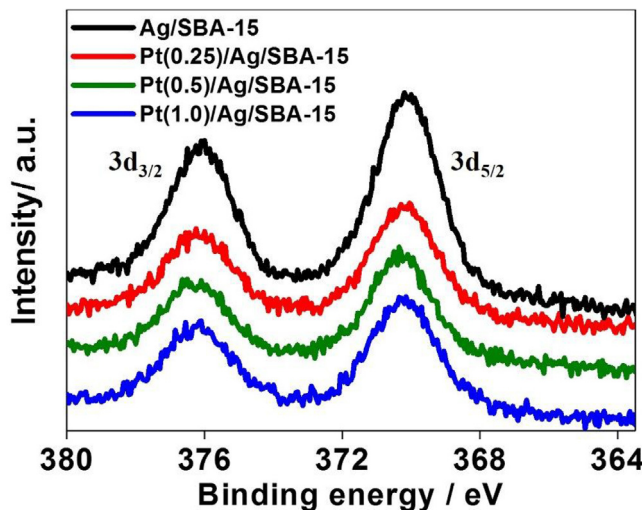


Fig. 4. XPS Ag 3d spectra for Ag/SBA-15 and Pt(x)/Ag/SBA-15 ($x = 0.25, 0.5$ and 1.0).

3.1.5. XPS analysis

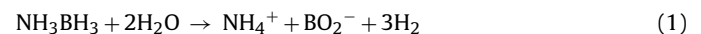
The X-ray photoelectron spectroscopy (XPS) measurement spectra for Ag/SBA-15 and Pt(x)/Ag/SBA-15, to characterize the surface composition and chemical state of prepared samples has been summarized in Fig. 4. The Ag 3d core level spectrum representing two strong peaks due to the splitting of 3d doublet by 6.0 eV confirms the metallic nature of Ag. The peaks observed at binding energies of 376.1 eV and 370.1 eV are ascribed to $3d_{3/2}$ and $3d_{5/2}$ core levels of Ag in Ag/SBA-15 respectively. We observed a successive shift by 0.1 eV for Pt (0.25), Pt (0.5) and Pt(1.0)/Ag/SBA-15 samples towards higher binding energies. The shift in the binding energy of Pt/Ag towards higher values in comparison to the monometallic Ag NPs implies the oxidation of Ag, owing to the net charge transfer from Ag to Pt. This transfer from Ag atoms and making electron rich Pt species, occurs due to the net difference in their electronegativity values (Ag: 1.93 and Pt: 2.28). Similarly, the spectral peaks of Pt 4f showed shift in the low binding energies for Pt(1.0)/Ag/SBA-15 in comparison to Pt/SBA-15 and hence becoming more electron rich (Fig. S4). It was difficult to observe intense

peaks for Pt loading of less than 1 wt% on Ag. Thus, XPS provides an advantage to display the existence of heterojunction via electron transfer mechanisms situated adjacent to each other.

3.2. Catalytic reaction

3.2.1. Ammonia borane dehydrogenation

The hydrogen production from AB can takes place via two processes viz. pyrolysis and hydrolysis. Pyrolysis takes place at considerably higher temperatures and produces only 1 equivalent of hydrogen (6.5 wt%), whereas hydrolysis in the presence of suitable catalyst yields 3 equivalents (19.6 wt%) of hydrogen as per Eq. (1) [34].



Among various investigated cases of AB hydrolysis in homogeneous and heterogeneous systems, various different catalysts have been well explored and reported. Apart from monometallic catalysts like Ag, Au, Ru, Rh and Pt, various bimetallic and trimetallic combinations have also been explored, for example, Pd/Ag, Pd/Au, RuNi, PtRh, RuCo, PtNiAu have been reported in the literature [35–37].

Fig. 5 summarizes the results obtained in the present study utilizing Pt(x)/Ag/SBA-15 bimetallic catalyst with varying ratio of Pt deposited on Ag. The time profile plots of hydrogen production for all catalysts is shown in Fig. S5. It was found out that on increasing the Pt wt% on Ag, the catalytic activity was also increased, attaining saturation at 1:1 (Pt: Ag) wt% ratio with a reaction rate of $1.16 \mu\text{mol min}^{-1}$. The highest reaction rate of $1.26 \mu\text{mol min}^{-1}$ was shown by Pt(0.5)/Ag/SBA-15 while a decreased rate for Pt(1.0)/Ag/SBA-15 ($1.16 \mu\text{mol min}^{-1}$) was observed under dark conditions. All catalysts showed an enhanced rate under visible light irradiation with highest rate of $1.69 \mu\text{mol min}^{-1}$ shown by Pt(1.0)/Ag/SBA-15. However, the enhancement extent was found to be maximum for 0.25 wt% of Pt on Ag. Enhancement factor (R_L/R_D) was calculated to study the differences in the rate of the reaction in dark and light condition by the simple division of reaction rate under light (R_L) and dark (R_D) conditions.

The enhancement factor for Pt(0.25)/Ag/SBA-15 was found to be 2.88. This observed enhancement is also the highest ever from our previously reported results of monometallic and bimetallic sphero-

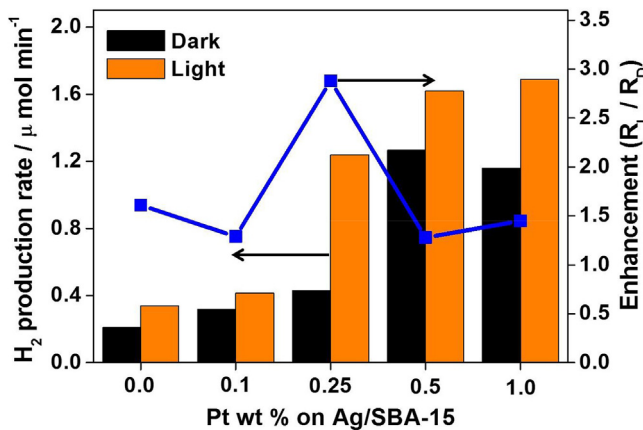


Fig. 5. Catalytic activity and corresponding enhancements for Ag/SBA-15 and Pt(x)/Ag/SBA-15 where x = 0.1, 0.25, 0.5 and 1.0.

ical NPs [13,14,25]. This enhancement can be attributed to the synergistic catalysis and optimum ratio of Pt (0.25) on Ag (1.0), giving rise to unique catalytic activity under light irradiation conditions for hydrogen production reaction. Two more catalysts were also prepared to study the trend of catalytic activity and corresponding enhancements by varying the Pt wt% ratio between 0.15 and 0.35 on Ag. The obtained results are shown in Fig. S6 displaying the maximum enhancement for 0.25 wt% of Pt on Ag. SBA-15 played an important role in designing the small sized Ag NPs within the channels of mesoporous silica. However, being completely transparent to UV-vis light, it has no special role in the enhanced activity in dark and under visible light irradiation.

3.2.2. Effect of light and temperature

The on/off effect of light irradiation was studied utilizing Pt(0.25)/Ag/SBA-15 catalyst for AB dehydrogenation as summarized in Fig. 6A. In the beginning, the catalytic activity was monitored for initial 30 min under dark conditions, followed by light irradiation for the next 60 min. It was observed a sudden increase in the reaction rate under visible light irradiation on switching from light off to on condition. Also, the slope of the activity curve found to be the same as that of activity monitored under light irradiation from 0 min. A significant enhancement after light irradiation validates the plasmonic effect of prepared catalyst.

Light originating from Xe lamp contains portions of visible and infrared light. It can be argued that the enhancements might be occurring due to the thermal effects arising from infrared light. Therefore, thermal reaction was carried out to study the effect of

heating by infrared light. As shown in Fig. 6B, the reaction rate of thermal reaction was found to be 0.65 μmol min⁻¹, which is higher than dark conditions (0.43 μmol min⁻¹) but significantly lower than that of light irradiation conditions (1.24 μmol min⁻¹). Hence, it can be concluded that the enhanced reaction rate essentially arises from the LSPR effect of Ag NPs. This has already been evidenced by the Eq. (2) reported by Christopher et al.

$$T = T_{\infty} + \frac{I_0 K_{abs} r_0}{6 k_{\infty}} \quad (2)$$

Where I₀ is the light intensity, K_{abs} is the absorption efficiency, r₀ is the diameter of metallic NP, k_∞ is the thermal conductivity of the surrounding medium and T_∞ is the heating temperature. As per the above equation, the temperature increase due to plasmonic heating effect in present catalytic system was found to be less than 0.002 K upon inserting experimental values I₀ = 320 mW cm⁻², r₀ = 4–50 nm, T_∞ = 298 K and the values calculated by Christopher et al. (K_{abs} = 3, k_∞ = 40 mW m⁻¹ K⁻¹) [38].

3.2.3. Stability test

Stability and recycling ability play an important role in order to design an active and efficient catalyst. The stability of Pt(0.25)/Ag/SBA-15 was investigated by carrying out recycling experiments under dark and visible light irradiation. In every successive cycle, AB was injected again and catalytic activity was monitored by using GC. As shown in Fig. S7, the reaction rate of 1.24 μmol min⁻¹ was found to be consistent enough under light irradiation conditions. The catalytic activity still remained high even after 3rd run, indicating the stability of the prepared catalyst.

3.2.4. Mechanism

A plausible mechanism involving the tentative reaction pathway has been proposed to understand the enhanced reaction rate under visible light irradiation. Upon light irradiation, the electron hole pairs are generated as per non-radiative Landau damping phenomenon for metal NPs of diameter equal to or less than 30 nm [39]. The plasmonic or the hot electrons generated due to resonant excitation undergoes possible relaxation within 0.5–1 ps [40]. The positioning of the fermi level of Pt lower to that of Ag leads to the net electron transfer from Ag to Pt as illustrated in Scheme 1. This process occurs due to substantial lower work function values of Ag (4.3 eV) than Pt (5.4 eV) from vacuum [41]. The hot electrons further injected to the lowest unoccupied molecular orbital (LUMO) of the reactant molecules to generate ionic species leading to their bond elongation [42]. The electrons tentatively further return back to plasmonic NPs via highest occupied molecular orbital (HOMO). After the activation of the reactant molecules, the electrons return

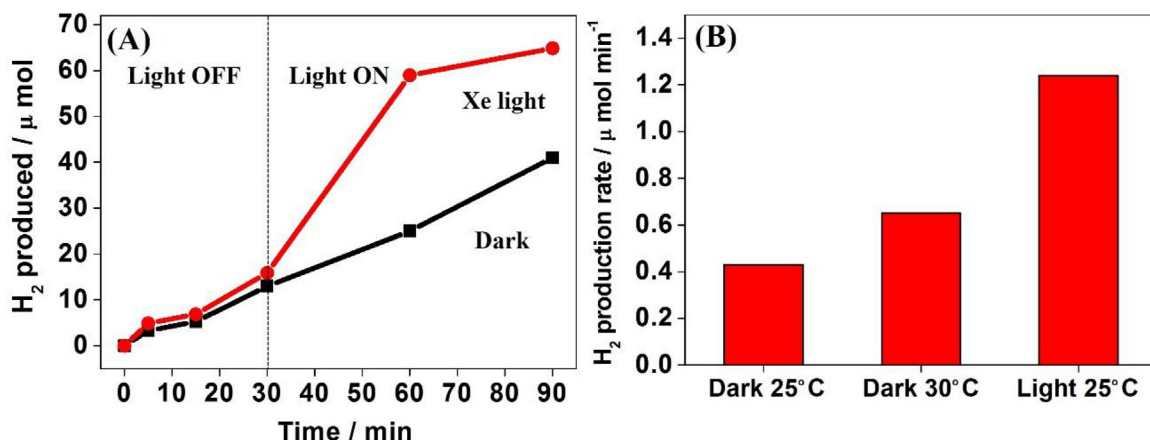
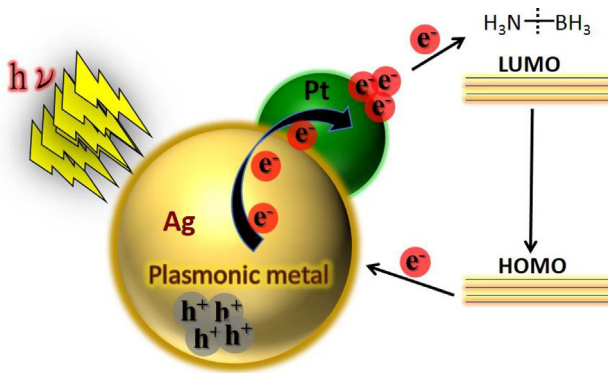


Fig. 6. (A) Off-on effect of light irradiation and (B) Effect of temperature under dark and light irradiation for AB dehydrogenation using Pt(0.25)/Ag/SBA-15.



Scheme 1. Illustration of the Pt/Ag system and possible electron transfer pathway for AB dehydrogenation under visible light irradiation.

to the HOMO and ultimately back to the plasmonic metal NPs and undergo recombination [43,44]. The confirmation of bond weakening or elongation under irradiation conditions based on the theoretical DFT calculations has also been reported by Q. Xiao et al. [42]. Many theoretical and calculative studies have also proved and reported the similar pathway followed by plasmonic metal NPs.

4. Conclusion

In summary, we have developed a Pt/Ag bimetallic plasmonic nanocatalyst supported within the channels of mesoporous silica. By varying the ratio of Pt on Ag, 0.25 wt% of Pt on Ag (1.0 wt%) was found to exhibit maximum enhancement (2.88) and superior catalytic activity with a reaction rate of $1.24 \mu\text{mol min}^{-1}$. The enhanced reaction rate under visible light irradiation has been demonstrated by proposing a tentative electron pathway for the AB dehydrogenation reaction. The effects of temperature and light were also carefully studied and explained, in order to elucidate the effect of thermal infrared heating. We hope that such development and advancements of LSPR-assisted catalysis will surely impact large scale energy and environmental aspects in the upcoming years.

Acknowledgements

The present work was partially supported by Grants-in-Aid for Scientific Research (Nos. 26220911, 26630409, 26620194, and T16K14478) from the Japan Society for the Promotion of Science (JSPS) and MEXT. We acknowledge Dr. Eiji Taguchi and Prof. H. Yasuda at the Research Center for Ultra-High Voltage Electron Microscopy, Osaka University, for their assistance with the TEM measurements. YK, KM and HY thank MEXT program “Elements Strategy Initiative to Form Core Research Center”. PV would like to acknowledge Japan International Corporation Agency (JICA) for research fellowship (D-14-90271).

Appendix A. Supplementary data

Supplementary data associated with this article can be found, in the online version, at <http://dx.doi.org/10.1016/j.apcatb.2017.05.017>.

References

- [1] J.N. Anker, W.P. Hall, O. Lyandres, N.C. Shah, J. Zhao, R.P. Van Duyne, *Nat. Mater.* 7 (2008) 442–453.
- [2] P.R. West, S. Ishii, G.V. Naik, N.K. Emani, V.M. Shalaev, A. Boltasseva, *Laser Photonics Rev.* 4 (2010) 795–808.
- [3] (a) H. Cheng, M. Wen, X. Ma, Y. Kuwahara, K. Mori, Y. Dai, B. Huang, H. Yamashita, *J. Am. Chem. Soc.* 138 (2016) 9316–9324;
(b) H. Cheng, X. Qian, Y. Kuwahara, K. Mori, H. Yamashita, *J. Mater. Chem. A* 27 (2015) 4616–4621;
(c) X. Meng, L. Liu, S. Ouyang, H. Xu, D. Wang, N. Zhao, J. Ye, *Adv. Mater.* 28 (2016) 6781–6803.
- [4] S. Gwo, C.-Y. Wang, H.-Y. Chen, M.-H. Lin, L. Sun, X. Li, W.-L. Chen, Y.-M. Chang, H. Ahn, *ACS Photonics* 3 (2016) 1371–1384.
- [5] M.E. Stewart, C.R. Anderton, L.B. Thompson, J. Maria, S.K. Gray, J.A. Rogers, R.G. Nuzzo, *Chem. Rev.* 108 (2008) 494–521.
- [6] V.K. Valev, D. Denkova, X. Zheng, A.I. Kuznetsov, C. Reinhardt, B.N. Chichkov, G. Tsutsumanova, E.J. Osley, V. Petkov, B. De Clercq, A.V. Silhanek, Y. Jeyaram, V. Volskiy, P.A. Warburton, G.A.E. Vandembosch, S. Russev, O.A. Aktsipetrov, M. Ameloot, V.V. Moshchalkov, T. Verbiest, *Adv. Mater.* 24 (2012) 29–35.
- [7] (a) C.H. Chou, F.C. Chen, *Nanoscale* 6 (2014) 8444–8458;
(b) H.A. Atwater, A. Polman, *Nat. Mater.* 9 (2010) 865.
- [8] X. Zheng, L. Zhang, *Energy Environ. Sci.* 9 (2016) 2511–2532.
- [9] (a) C. Ropers, D.J. Park, G. Stibenz, G. Steinmeyer, J. Kim, D.S. Kim, C. Lienau, *Phys. Rev. Lett.* 94 (2005) 113901–113905;
(b) P.K. Jain, X. Huang, I.H. El-Sayed, M.A. El-Sayed, *Plasmonics* 2 (2007) 107–118.
- [10] S. Linic, P. Christopher, D.B. Ingram, *Nat. Mater.* 10 (2011) 911–921.
- [11] M.L. Brongersma, N.J. Halas, P. Nordlander, *Nat. Nanotechnol.* 10 (2015) 25–34.
- [12] (a) S. Mukherjee, F. Libisch, N. Large, O. Neumann, L.V. Brown, J. Cheng, J.B. Lassiter, E.a. Carter, P. Nordlander, N.J. Halas, *Nano Lett.* 13 (2013) 240–247;
(b) M. Sun, H. Xu, *Small* 8 (2012) 2777–2786.
- [13] P. Verma, Y. Kuwahara, K. Mori, H. Yamashita, *J. Mater. Chem. A* 4 (2016) 10142–10150.
- [14] K. Fuku, R. Hayashi, S. Takakura, T. Kamegawa, K. Mori, H. Yamashita, *Angew. Chem. Int. Ed.* 52 (2013) 7446–7450.
- [15] M. Zhu, P. Chen, W. Ma, B. Lei, M. Liu, *ACS Appl. Mater. Interfaces* 4 (2012) 6386–6392.
- [16] R. Jin, Y.C. Cao, E. Hao, G.S. Métraux, G.C. Schatz, C. a Mirkin, *Nature* 425 (2003) 487–490.
- [17] (a) X. Lu, L. Au, J. McLellan, Z.Y. Li, M. Marquez, Y. Xia, *Nano Lett.* 7 (2007) 1764–1769;
(b) J. Zeng, Q. Zhang, J. Chen, Y. Xia, *Nano Lett.* 10 (2010) 30–35.
- [18] C. Zhang, B.-Q. Chen, Z.-Y. Li, Y. Xia, Y.-G. Chen, *J. Phys. Chem. C* 119 (2015) 16836–16845.
- [19] (a) K.J. Major, C. De, S.O. Obare, *Plasmonics* 4 (2009) 61–78;
(b) M. Zienkiewicz-Strzałka, A. Deryło-Marczewska, S. Pikus, *Microporous Mesoporous Mater.* 227 (2016) 228–241.
- [20] D. Manchon, J. Lermé, T. Zhang, A. Mosset, C. Jamois, C. Bonnet, J.-M. Rye, A. Belaroui, M. Broyer, M. Pellarin, E. Cottancin, *Nanoscale* 7 (2015) 1181–1192.
- [21] K. Baranowska, J. Okal, W. Tylus, *Appl. Catal. A Gen.* 511 (2016) 117–130.
- [22] S. Guo, D. Wen, Y. Zhai, S. Dong, E. Wang, *ACS Nano* 4 (2010) 3959–3968.
- [23] P. Verma, Y. Kuwahara, K. Mori, H. Yamashita, *J. Mater. Chem. A* 3 (2015) 18889–18897.
- [24] S.-S. Chang, C.-L. Lee, C.R.C. Wang, *J. Phys. Chem. B* 101 (1997) 6661–6664.
- [25] K. Mori, P. Verma, R. Hayashi, K. Fuku, H. Yamashita, *Chem. Eur. J.* 21 (2015) 11885–11893.
- [26] H. Lang, S. Maldonado, K.J. Stevenson, B.D. Chandler, *J. Am. Chem. Soc.* 126 (2004) 12949–12956.
- [27] U. Eberle, M. Felderhoff, F. Schuth, *Angew. Chem. Int. Ed.* 48 (2009) 6608–6630.
- [28] A.W.C. van den Berg, C.O. Areán, *Chem. Commun.* (2008) 668–681.
- [29] J. Yang, A. Sudik, C. Wolverton, D.J. Siegel, *Chem. Soc. Rev.* 39 (2010) 656–675.
- [30] E.K. Abo-Hamed, T. Pennycook, Y. Vaynzof, C. Toprakcioglu, A. Koutsoubas, O.A. Scherman, *Small* 10 (2014) 3145–3152.
- [31] D. Zhao, Q. Huo, J. Feng, B.F. Chmelka, G.D. Stucky, *J. Am. Chem. Soc.* 120 (1998) 6024–6036.
- [32] K. Mori, Y. Miura, S. Shironita, H. Yamashita, *Langmuir* 25 (2009) 11180–11187.
- [33] F. Liu, D. Wechsler, P. Zhang, *Chem. Phys. Lett.* 461 (2008) 254–259.
- [34] K. Mori, K. Miyawaki, H. Yamashita, *ACS Catal.* 6 (2016) 3128–3135.
- [35] (a) J. Kang, T. Chen, D. Zhang, L. Guo, *Nano Energy* 23 (2016) 145–152;
(b) M. Navlani-García, K. Mori, A. Nozaki, Y. Kuwahara, H. Yamashita, *Appl. Catal. A Gen.* 527 (2016) 45–52.
- [36] W. Zhan, Q.-L. Zhu, Q. Xu, *ACS Catal.* 6 (2016) 6892–6905.
- [37] Q. Wang, Z. Liu, W. Wang, D. Liu, W. Shi, J. He, P. Shao, R. Shi, F. Cui, *Int. J. Hydrogen Energy* 41 (2016) 8470–8478.
- [38] P. Christopher, H. Xin, S. Linic, *Nat. Chem.* 3 (2011) 467–472.
- [39] C. Burda, X. Chen, R. Narayanan, M.a. El-Sayed, *Chem. Rev.* 105 (2005) 1025–1102.
- [40] D.D. Evanoff, G. Chumanov, *ChemPhysChem* 6 (2005) 1221–1231.
- [41] S. Trasatti, *Electroanal. Chem. Interfacial Electrochem.* 33 (1971) 351–378.
- [42] Q. Xiao, S. Sarina, E. Jaatinen, J. Jia, D.P. Arnold, H. Liu, H. Zhu, *Green Chem.* 16 (2014) 4272–4285.
- [43] S. Linic, U. Aslam, C. Boerigter, M. Morabito, *Nat. Chem.* 14 (2015) 567–576.
- [44] P. Verma, Y. Kuwahara, K. Mori, H. Yamashita, *Chem. Eur. J.* 23 (2017) 3616–3622.